Philosophical Magazine
Vol. 00, No. 00, 00 Month 200x, 1–7

RESEARCH ARTICLE

On the structure of quasi-two-dimensional foams

S.J. Cox[a] *, and E. Janiaud[b]

[a]*Institute of Mathematics and Physics, Aberystwyth University, SY23 3BZ, UK*;
[b]*ESPCI, 10 rue Vauquelin, 75231 Paris Cedex 05, France*

(*Received 00 Month 200x; final version received 00 Month 200x*)

Bubble monolayers are widely used to probe the rheology of aqueous foams, and liquid content plays an important role in the response. We analyse the liquid distribution within three different types of two-dimensional foam, and predict (i) the rigidity loss transition in each case and (ii) the fraction of the bounding surfaces touched by the liquid network. The latter quantity allows the liquid fraction in an experiment to be determined non-invasively by image analysis.

Keywords: Two-dimensional foams, bubbles, liquid fraction

1. Introduction

Two-dimensional (2D) foams - that is, a single layer of bubbles - are often used in the laboratory in preference to "real" 3D foams. Being able to see every bubble gives a great advantage in being able to determine precisely the foam response and to relate foam properties to the microscopic structure.

However, 2D experiments are not actually 2D – we call them *quasi-2D*, because of the liquid network that surrounds the bubbles (figure 1). An exception is that of Langmuir monolayer foams [1, 2], which really are two-dimensional, but these are not used much in practice.

The liquid in a foam is concentrated in Plateau borders [3] and the vertices where they meet [4], and plays in important role in the rheology [5] and drainage [4] of foams. Quantities such as yield stress depend strongly upon the amount of liquid in the foam [6]. In particular, the liquid fraction, defined as the ratio of the volume of liquid to the total volume of the foam, probably controls the onset of convective motion [7] in draining foams [8], a process that for the theoretician links rheology with drainage and for the industrialist causes (usually) unwanted motion of the bubbles.

Thus, the first step in understanding the flow of, and liquid flow through, a foam, is to precisely define the liquid structure. There are three usual realizations of a 2D foam, illustrated in figure 1. We describe them using the notation of [5]:

- The glass-glass set-up ($\mathcal{GG}$) consists of a layer of bubbles between parallel glass (or perspex) plates (figure 1(a)) [9], i.e. in a Hele-Shaw cell [10]. Plateau borders are formed at the three-fold junctions between films and also where the

*Corresponding author. Email: foams@aber.ac.uk

ISSN: 1478-6435 print/ISSN 1478-6443 online

DOI: 10.1080/1478643YYxxxxxxxx
http://www.informaworld.com

films meet the plates. This is the set-up that allows the best control of the liquid fraction (which is well-defined), and, since the plates can be vertical as well as horizontal, it is possible to neglect the effects of gravity in a well-drained foam.

- The liquid-glass set-up ($\mathcal{LG}$) is one in which a layer of bubbles floats upon a liquid reservoir with a horizontal glass plate pressed down upon them (figure 1(b)) [11–13]. There is now a meniscus at the bottom of the foam, the height of which is determined by the capillary length, i.e. it depends upon the balance between surface tension and gravity. It is much more difficult to define a liquid fraction here, and instead some "effective" measure of the liquid content is required [14].
- The liquid-air set-up ($\mathcal{LA}$), or bubble raft, consists of a layer of bubbles floating on a liquid reservoir [15, 16]. It suffers from the same caveats as for $\mathcal{LG}$ experiments, but now the effect of gravity is even more apparent and the Plateau borders close to the tops of the bubbles are very small.

The purpose of this letter is to use 3D simulations with the Surface Evolver [17] to explore the effect of the liquid surrounding the bubbles. Our analysis is confined to static properties, since the computer simulation of flowing wet three-dimensional foams is still remarkably difficult. For each of the three systems described above, we are able to calculate the area of the films separating bubbles from each other and from the glass plates, as material parameters such as bubble size are varied. This allows us to give guidance to the experimentalist who wants to be able to assign a simple measure of effective liquid fraction to an experiment, and we indicate such a procedure below, improving upon the calculations used to produce fig 4. in [18]. It also allows us to predict the onset of structural changes, when bubbles become free enough to move as the liquid content increases.

2. Simulation method

We use the Surface Evolver [17] to study the bubble shape that occurs when the liquid fraction is not negligible. To simplify the problem further, we assume that all bubbles in the foam are identical hexagonswhen viewed from above, and therefore we can employ periodic boundary conditions on a single bubble to reduce computational time. We first create a dry periodic hexagonal structure, and then "decorate" it with liquid channels. The liquid surfaces are tessellated into a collection of triangles, and appropriate surface tensions applied to each one. Each computation then proceeds through a combination of sub-dividing small triangles and gradient descent steps. To obtain an accurate description of the surface we use 3 levels of refinement, resulting in a representation with up to 500,000 small triangular facets for the driest foams.

We scale all lengths by L, the edge length of the equivalent dry bubble (figure 1(d)). For convenience we choose cgs units with $L = 1$cm ($\mathcal{GG}$, $\mathcal{LG}$) or $L = 0.5$cm ($\mathcal{LA}$), and vary the plate separation D in the range 0.2cm to 1cm in steps of 0.1cm ($\mathcal{GG}$, $\mathcal{LG}$), the liquid fraction Φ ($\mathcal{GG}$) or the bubble volume V_b ($\mathcal{LA}$). Large aspect ratios D/L lead, in general, to an instability [19] that causes more than one layer of bubbles to be formed; although a hexagonal foam is (atypically) unconditionally stable in this respect, we choose $D \leq L$ for its more general relevance. The area of the unit cell when viewed from above is $A_p = 3\sqrt{3}/2L^2$ and its total volume equal to $V = A_p D$. When a liquid pool is present, the total volume of liquid is zero, i.e. the total volume of liquid in the Plateau borders is equal to the volume of gas below the undisturbed water level.

The surface tension of the liquid air interface is taken as $\gamma_{la} = 25\text{g s}^{-2}$. The

surface tension of the thin films should be close to twice this value: to represent the disjoining pressure in the films, we choose $\gamma_{film} = 49.5$ g s^{-2}. We find that the difference $2\gamma_{la} - \gamma_{film}$ can be varied without having a significant effect on the foam structure (compared to, say, equivalent changes in plate separation), see below. We take the liquid density to be $\rho = 1$g cm^{-3}, and the acceleration due to gravity to be $g = 981$cm s^{-2}. The capillary length, $\ell_c = \sqrt{\gamma_{la}/\rho g}$, is equal to 0.16cm.

From each simulation we extract (i) the area A_v of each of the inter-bubble (vertical) soap films, and (ii) the area A_h of each of the soap films in contact with the glass plates ($\mathcal{GG}$, $\mathcal{LG}$).

3. Simulation results

We tackle the case $\mathcal{GG}$ in the absence of gravity: since this is a closed system the liquid fraction and bubble size can be chosen independently and we therefore give results in terms of the actual liquid fraction and plate separation D/L. For the other two cases, gravity is included and there is only one variable, the separation D/L ($\mathcal{LG}$) or bubble volume V_b/L^3 ($\mathcal{LG}$).

3.1. *Inter-bubble film area and the rigidity loss transition*

We show in figure 2(a) how the area A_v of the soap films that separate two bubbles in the case $\mathcal{GG}$ shrinks with increasing Φ, at fixed D/L, and with decreasing D/L at fixed Φ. We refer to these as vertical films, in analogy with the other two set-ups.

The largest values of Φ used are those for which, for each value of the separation D, the vertical films shrink to zero area. This critical value Φ_c signals the rigidity loss transition [20] at which bubbles start to move independently. Our calculations show (figure 2(a)) that Φ_c increases with D/L in an affine manner [21].

For the $\mathcal{LG}$ case, figure 2(b) shows that A_v goes to zero when $D \approx 0.23L$, and in the $\mathcal{LA}$ case, figure 2(c) shows that A_v goes to zero when $V_b \approx 1.27L^3$.

3.2. *Wetted area*

We wish to relate the actual liquid fraction Φ to some external measure of the shape of the surface, to facilitate the job of the experimentalist in determining liquid fraction from an external observation (e.g. a photograph). We therefore recorded the visible area of each bubble A_h in the cases where there is a glass plate present, which is possible to obtain from an experiment by image analysis. From this we calculate the wetted fraction of one of the confining plates: $A_w/A_p = 1 - A_h/A_p$, where A_p is the area of the glass plate. This quantity, shown in figure 3, increases with increasing liquid content.

The effect of increasing the disjoining pressure, defined as the normalized difference between the surface tensions of film and Plateau border, is to reduce the wetted fraction by increasing the contact angle between glass and liquid. In principle, a comparison of the data in figures 3(a) and 3(c) should allow us to define an effective liquid fraction for the case $\mathcal{LG}$.

To give a rule of thumb, we fit the data for the wetted fraction in the $\mathcal{GG}$ case, from figure 3(a), to a power law form (omitting the data for $D/L \leq 0.2$):

$$\Phi = f(A_w/A_p; D/L) = \alpha(A_w/A_p)^\beta. \tag{1}$$

The result is shown in figure 3(b). We find that the exponent β is constant, $\beta =$

2.449 ± 0.005; the prefactor α depends upon the separation D/L, in the form $\alpha = \alpha_0 (D/L)^{-\alpha_1}$ with $\alpha_0 = 0.590 \pm 0.006$ and $\alpha_1 = 1.177 \pm 0.011$. Thus,

$$f(A_w/A_p; D/L) \approx 0.59 \left(\frac{D}{L}\right)^{-1.18} \left(\frac{A_w}{A_p}\right)^{2.45} . \quad (2)$$

We show the collapse of the data in the inset to figure 3(b).

4. Experimental validation

We provide here evidence from experiment that the form (2) is appropriate. We used a commercial dishwashing liquid (Fairy liquid) at a concentration of 2.5% by volume to stabilize a foam whose bubble edge length L was of millimetric size. The foam was confined between two vertical glass plates forming a Hele-Shaw cell 5cm wide and 42 cm high with separation $D = 1.5$mm. The bottoms of the plates were immersed in a liquid pool. The liquid fraction Φ was varied by adding liquid to the top of the foam at a steady flow rate. Pictures were recorded at about 30 cm below the liquid injection point to ensure uniform volume fraction.

The foam was lit with a set-up following the principle of an overhead projector, in which a nearly parallel beam crosses the foam and is projected onto a screen using a convergent lens. Plateau borders are clearly distinguished because curved interfaces diffract light. A firewire CCD camera connected to a computer recorded the pictures. Grey levels were thresholded and each picture binarized in order separate wetted area from the rest of the picture. Wetted fraction and bubble edge length were measured with a homemade plugin for ImageJ [22]. A second camera recorded the distance h between the bottom of the foam and the surface of the liquid pool. Assuming that the weight of the foam is balanced by Archimedes' force, the average volume fraction is simply given by the ratio of h to the total height of the foam.

We find that the data obtained for various D/L (figure 4) collapses to a line when plotted using (2), at least partially validating the simulations. The slope depends on the inherently arbitrary threshold during image processing and was found to range between 0.6 and 0.8 (0.66 in figure 4) and is thus always smaller than unity. This could be explained by optical problems inherent in looking through wet glass, which would lead to an underestimation of the volume fraction [23]. Other possible explanations for the discrepancy between experiments and simulations could be an underestimation of the weight of the foam due to the viscous drag of the soap films on the glass or their pinning, or it could be due to the different surface tension or disjoining pressure between simulation and experiment, since this has not been measured in the latter.

5. Summary

We have shown that simulations such as those described here can describe the liquid distribution in experiments on so-called 2D foams. This generates rule-of-thumb predictions to allow the experimentalist to relate surface observations to bulk properties. In the future, we hope to be able to provide more precise measures of effective liquid fraction, which may be helped by our ability to extract the mean curvature of the Plateau border surfaces.

The predictions given here may have a dependence upon the capillary number and the bubble size. Although this is expected to be small, the dependence of

wetted fraction upon disjoining pressure in figure 3(c) suggests that such a study may be of interest.

Further benefit will be gained from the analysis of images of horizontal slices through the simulated foams, which could be compared with real data obtained with confocal microscopy, therefore reducing the problems of refraction and pinning at the interface between the foam and the bounding plates. Such data is now becoming available in the Hele-Shaw case from 2-photon microscopy [24].

Acknowledgements

For many years what we have termed the liquid-glass method was synonymous with the name of Manuel Fortes and the work of the Lisbon group. Manuel's enthusiasm and his prolific ideas will be missed.

We thank K. Brakke for his development and maintenance of the Surface Evolver code, I. Cantat, N. Denkov and F. Graner for their insightful comments on this work, and the participants in the Grenoble Foam Mechanics Workshop (2008) for their suggestions. EJ thanks D. Weaire and S. Hutzler for support, and ESA (MAP AO-99-108:C14914/02/NL/SH, MAP AO-99-075:C14308/00/NL/SH) for funding. SJC thanks the British Council Alliance programme, CNRS and EPSRC (EP/D048397/1, EP/D071127/1) for financial support.

References

[1] M. Lösche, E. Sackmann, and H. Möhwald. A fluorescence microscopic study concerning the phase diagram of phospholipids. *Ber. Bunsenges. Phys. Chem.*, **87**:848–852, 1983.

[2] B. Berge, A.J. Simon, and A. Libchaber. Dynamics of gas bubbles in monolayers. *Phys. Rev. A*, **41**:6893–6900, 1990.

[3] J.A.F. Plateau. *Statique Expérimentale et Théorique des Liquides Soumis aux Seules Forces Moléculaires*. Gauthier-Villars, Paris, 1873.

[4] D. Weaire and S. Hutzler. *The Physics of Foams*. Clarendon Press, Oxford, 1999.

[5] M.F. Vaz and S.J. Cox. Two-bubble instabilities in quasi-two-dimensional foams. *Phil. Mag. Letts.*, **85**:415–425, 2005.

[6] H.M. Princen. Rheology of Foams and Highly Concentrated Emulsions. I. Elastic Properties and Yield Stress of a Cylindrical Model System. *J. Coll. Int. Sci.*, **91**:160–174, 1983.

[7] S. Hutzler, D. Weaire, and R. Crawford. Convective instability in foam drainage. *Europhysics Lett.*, **41**:461–465, 1998.

[8] S. Hutzler, S.J. Cox, E. Janiaud, and D. Weaire. Drainage induced convection rolls in foams. *Coll. Surf. A*, **309**:33–37, 2007.

[9] G. Debrégeas, H. Tabuteau, and J.M. di Meglio. Deformation and flow of a two-dimensional foam under continuous shear. *Phys. Rev. Lett.*, **87**:178305, 2001.

[10] H.S. Hele-Shaw. The Flow of Water. *Nature*, **58**:34–36, 1898.

[11] C.S. Smith. Grain shapes and other metallurgical applications of topology. In *Metal Interfaces*, pages 65–108. American Society for Metals, Cleveland, OH, 1952.

[12] M.F. Vaz and M.A. Fortes. Experiments on defect spreading in hexagonal foams. *J. Phys.: Condens. Matt.*, **9**:8921–8935, 1997.

[13] B. Dollet, F. Elias, C. Quilliet, C. Raufaste, M. Aubouy, and F. Graner. Two-dimensional flow of foam around an obstacle: Force measurements. *Phys. Rev. E*, **71**:031403, 2005.

[14] C. Raufaste, B. Dollet, S. Cox, Y. Jiang, and F. Graner. Yield drag in a two-dimensional foam flow around a circular obstacle: Effect of liquid fraction. *Euro. Phys. J. E*, **23**:217–228, 2007.

[15] L. Bragg and J.F. Nye. A dynamical model of a crystal structure. *Proc. R. Soc. Lond.*, A**190**:474–481, 1947.

[16] J. Lauridsen, M. Twardos, and M. Dennin. Shear-induced stress relaxation in a two-dimensional wet foam. *Phys. Rev. Lett.*, **89**:098303, 2002.

[17] K. Brakke. The Surface Evolver. *Exp. Math.*, **1**:141–165, 1992.

[18] B. Dollet and F. Graner. Two-dimensional flow of foam around a circular obstacle: local measurements of elasticity, plasticity and flow. *J. Fl. Mech.*, **585**:181–211, 2006.

[19] S.J. Cox, D. Weaire, and M.F. Vaz. The transition from two-dimensional to three-dimensional foam structures. *Eur. Phys. J. E*, **7**:311–315, 2002.

[20] D. Weaire and F. Bolton. Rigidity Loss Transition in a Disordered 2D Froth. *Phys. Rev. Lett.*, **65**:3449, 1990.

[21] Following a suggestion by I. Cantat, we also recorded the width w_v of the inter-bubble films, in the sense parallel to the liquid surface, which may give a better measure of film extent for small aspect ratios D/L. In the present study although w_v/L saturates to one at low liquid content, we gain no new information about the rigidity loss transition: the values of A_v and w_v go to zero together.

[22] W.S. Rasband. *ImageJ*. U.S. National Institutes of Health, Bethesda, Maryland, USA, 1997–2007. http://rsb.info.nih.gov/ij/.

[23] A. van der Net, L. Blondel, A. Saugey, and W. Drenckhan. Simulating and interpreting images of foams with computational ray-tracing techniques. *Coll. Surf. A*, **309**:159–176, 2007.

[24] J.-P. Raven. *Generation, flow and manipulation of a microfoam*. PhD thesis, Université Joseph Fourier - Grenoble I, 2007. Chapter 2.

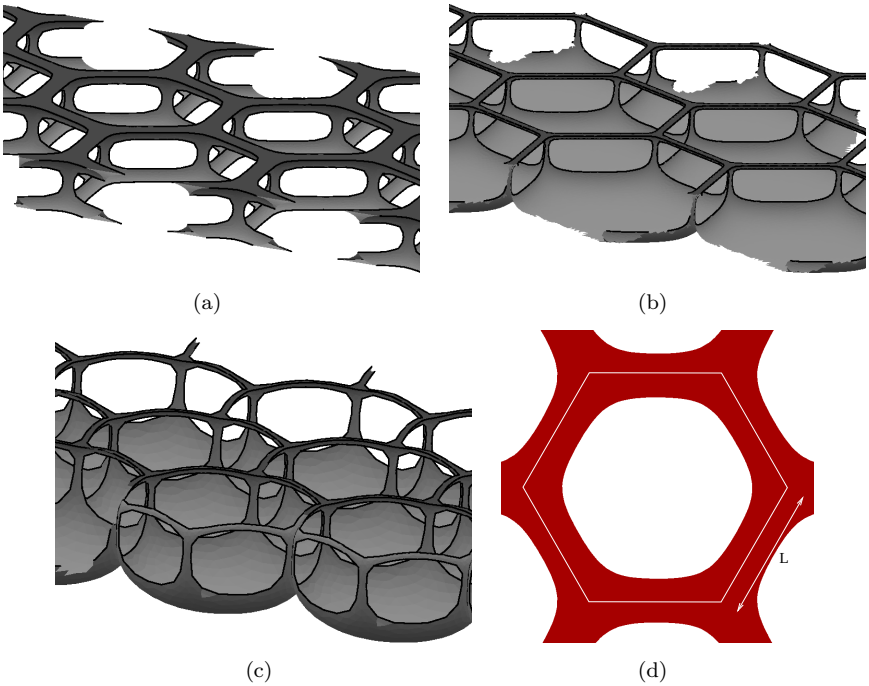

Figure 1. Oblique view of simulated quasi-2D hexagonal foams, from which the films have been removed for clarity. (a) Bubbles between parallel plates, $\mathcal{GG}$. (b) Bubbles between a liquid reservoir and a horizontal plate, $\mathcal{LG}$. (c) Bubbles floating on a liquid reservoir, $\mathcal{LA}$. (d) Plan view of the single repeated simulation unit that consists of a hexagonal bubble (outlined in white) and its associated liquid.

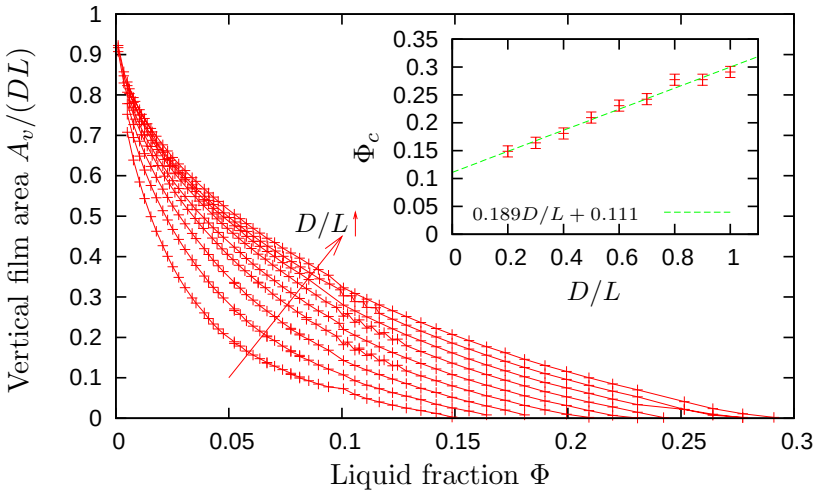

(a)

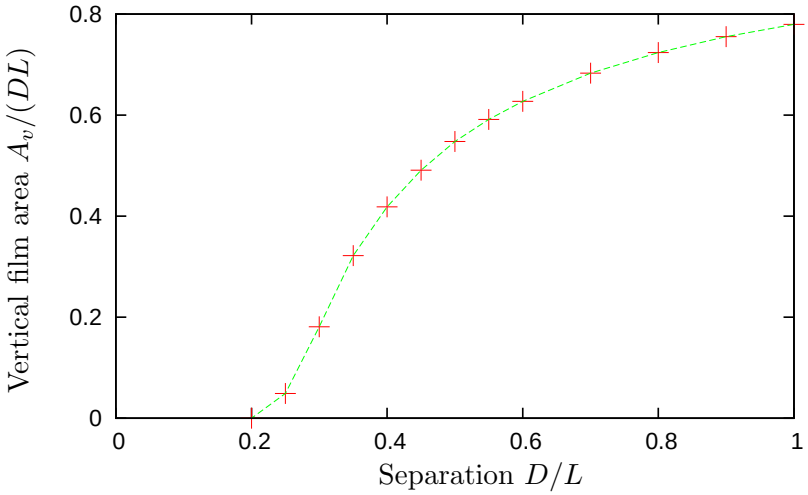

(b)

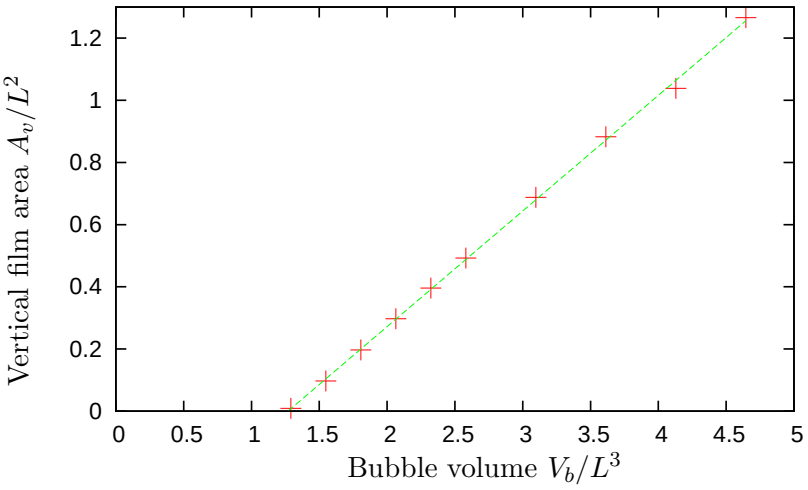

(c)

Figure 2. (a) The normalized area A_v of the vertical films separating neighbouring bubbles decreases with increasing liquid fraction for $\mathcal{GG}$. Each line represents a different value of plate separation D/L, increasing from 0.2 to 1 in steps of 0.1. The inset shows the critical value of Φ_c, the rigidity loss transition, at which the film area goes to zero. This decreases linearly with decreasing D/L. (b) In the $\mathcal{LG}$ case, the vertical films again shrink as the plate-liquid separation D/L is decreased. When $D/L \approx 0.23$ the rigidity loss transition is reached and the vertical films disappear. (c) In the $\mathcal{LA}$ case, the film area shrinks affinely with normalized bubble volume (the dotted line is a fit), and goes to zero when $V_b \approx 1.27L^3$. Note that the normalization of film area by L^2 is not quite appropriate, in that the ordinate scale exceeds one.

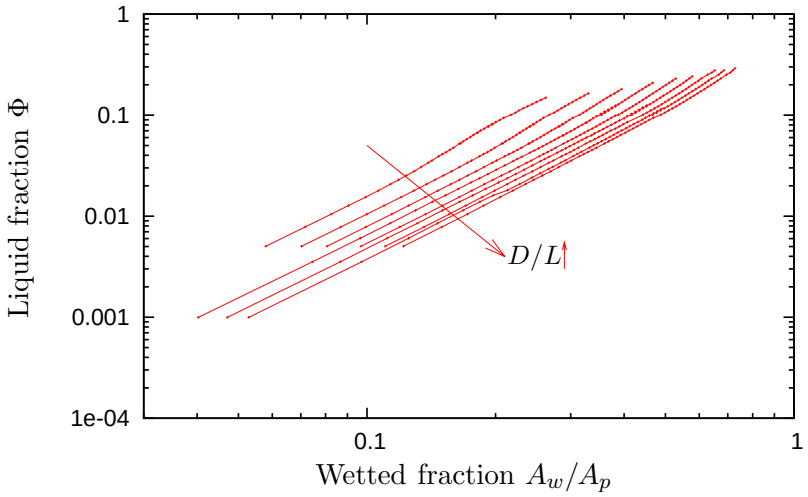

(a)

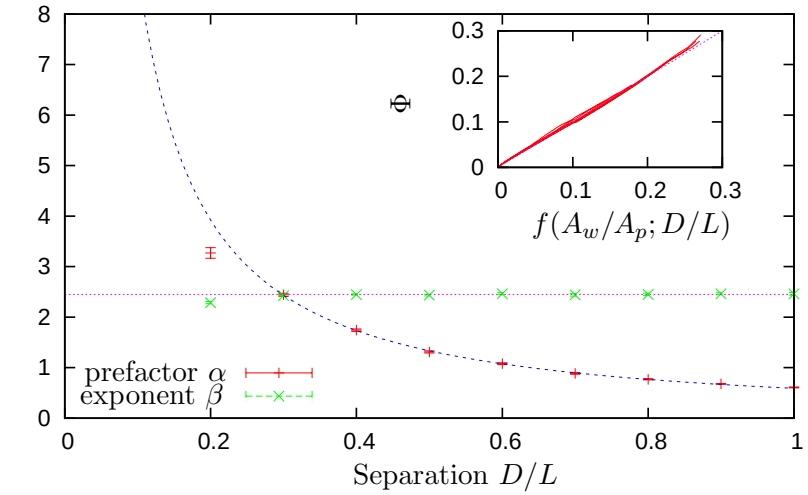

(b)

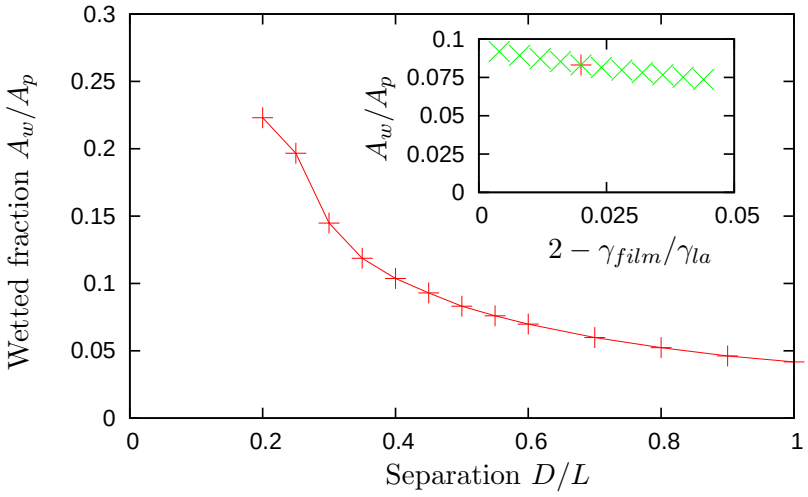

(c)

Figure 3. The fraction of the confining plates covered by liquid in the Plateau border network A_w/A_p. (a) The $\mathcal{GG}$ case, for different values of D/L between 0.2 and 1, on log scales, as a function of Φ. (b) The relationship between the liquid fraction Φ and the wetted fraction A_w/A_p, from (a), fits well to a power law form (1). Here we show the fitting parameters α and β, the power law fit for α and, in the inset, the rescaled data. (c) The $\mathcal{LG}$ case, for the same range of D/L. In the inset, we show the variation in A_w/A_p with (normalized) disjoining pressure for $D/L = 0.5$.

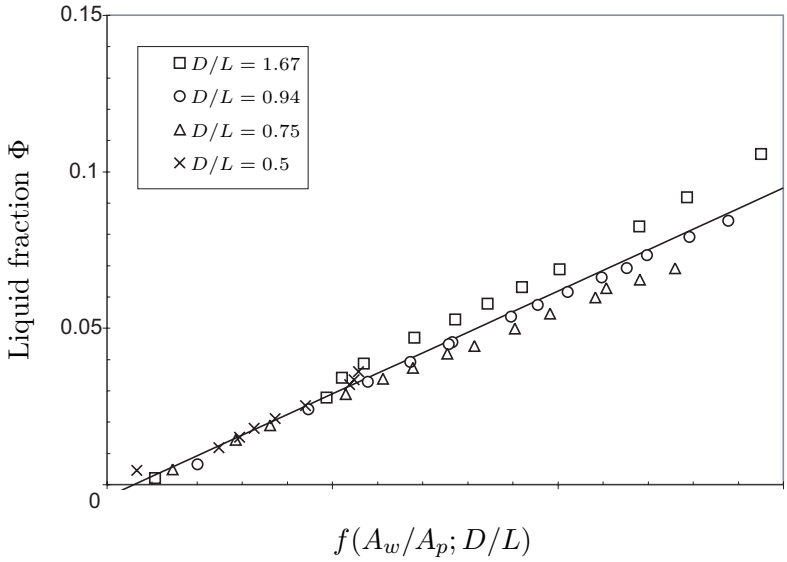

Figure 4. Experimental data for bubbles in a Hele-Shaw cell with various side-lengths L. The liquid fraction is calculated by weighing the foam, and compared with the prediction (2). The data collapses well to a line, but the slope of this line with equation $\Phi = 0.66f - 0.004$.